REKAYASAMESIN
eISSN 2477-6041 artikel 27, pp. 899 – 910, 2022
V13 N3

EFFECT OF SHIELDING GAS ON THE PROPERTIES OF STAINLESS-STEEL SUS 304L PLUG WELDED

Ilham Habibi
Tenaga Pengajar (Dosen)
Universitas Muhammadiyah Magelang
Jurusan mesin otomotif
habibi@unimma.ac.id

Januar Tri Prasetyo
Mahasiswa
Universitas sebelas maret
Jurusan teknik mesin

Nurul Muhayat
Tenaga Pengajar (Dosen)
Universitas sebelas maret
Jurusan teknik mesin

Triyono
Tenaga Pengajar (Dosen)
Universitas sebelas maret
Jurusan teknik mesin
triyono74@staff.uns.ac.id

The effect of shielding gas composition and welding current on the mechanical-physical properties of plug welding joint stainless steel SUS 304L has been investigated. Metal Inert Gas (MIG) welding was used to join SUS304L with a thickness of 3 mm. The variations of welding current were 80 A, 100 A, and 120 A, while variations of shielding gas composition were 100% Ar; 92,5% Ar-7,5% CO_2; 85% Ar-15% CO_2; 77,5% Ar-22,5% CO_2; 100% CO_2. Macro and microstructural tests were conducted to determine welded joints physical properties. Tensile-shear testing and micro hardness Vickers were done to determine welded joints physical properties. The results show that the higher level of welding current and CO_2 content in the shielding gas, the more tensile-shear load bearing capacity and decreased hardness. The welding current of 120 A and shielding gas 77,5% Ar-22,5% CO_2 produced welded joints with the highest tensile-shear load bearing capacity. The nugget size increased as the higher level of welding current and the CO_2 content in the shielding gas due to the increase of heat input.

Keywords: *MIG Welding, Plug Welding, Shielding Gas, Argon Gas, CO_2 Gas, Stainless Steel*

1. INTRODUCTION

Several industries such as the automotive industry, shipping industry and the railroad industry require a good metal joining process [1]. The best metal joining process is the welding process because joining process reaches the metal structure.Welding is an important part of industrial growth, because it plays an important role in construction sector [2]–[4]. Most modern industries always involve welding processes which are increasing every year.

Gas metal arc welding is often used in the manufacturing industry because of the many advantages of using shielding gas. Shielding gas is blown into the weld area to protect the arc and molten metal against the atmosphere [5]. In its development, gas arc welding is divided into several groups, one of those is MIG (Metal Inert Gas) welding [6]. MIG welding is arc welding that uses noble gases as a shield gas in welding process. MIG welding has several advantages in terms of efficiency, arc concentration and toughness, therefore MIG welding is widely used for welding high quality steel such as stainless steel [7].

Stainless steel is widely used as a construction material because it is corrosion resistant, easy to shape and can be welded. Type 304L stainless steel is widely used in industry, because this material has good forming and welding characteristics. SS340L has composition of (in %wt) 0,027% C; 0,39% Si; 1,61% Mn; 0,025% P; 0,011% S; 8,01% Ni; 18,27% Cr and 69,24% Fe [8]. The high chromium content of SUS304L forms a protective layer of chromium oxide to increase corrosion resistance [9]. Lower carbon content than SUS304 (0,042% to 0,027%wt) [10] minimizes carbide formation.

In the construction sector, the thin plate joint structure consists of a frame and sheet [11]. The frame is a reinforcement and sheet is a reinforced plate [12]. The joining process that is often used is spot welding or resistance spot welding. In its development, it is often found that there are problems with spot welding for joining metals with complicated profiles. Therefore, to improve the joint quality and overcome these obstacles, the joining process by spot welding is replaced by plug welding.

Plug weld is used to join two metals by welding, the top plate is perforated and then filled with welds. The result of this process resembles a spot weld with a circle shape. The plug weld method is carried out using MIG (Metal Inert Gas) or GMAW (Gas Metal Arc Welding) welding. Shielding gas in GMAW serves to protect weld metal and heat affected zone (HAZ) from oxidation and other contamination [13]. Shielding gas made from noble

Corresponding Author: triyono74@staff.uns.ac.id Received on: May 2022 Accepted on: July 2022
DOI: https://doi.org/10.21776/jrm.v13i3.1251

gases, which is 97% argon for thin plates and 100% helium for thick plates [14]. In the present time, researchers have started to use CO_2 as an alternative to shielding gas, some are pure CO_2 and some are a mixture of noble gas and CO_2 [9].

The plug welding process at MIG generally uses pure argon as shielding gas. In the market, the price of argon is relatively expensive, therefore, many variations of the shield gas have been studied with a mixture composition of Ar and CO_2 [15]. CO_2 is cheaper than Ar so it can reduce production costs [9]. Shielding gas mixed with CO_2 affects the mechanical properties of the weld [16]. This study aims to determine the most optimal welding current and shielding gas composition for welding results.

2. MATERIALS AND METHOD

Welding were done using a MIG-250 welding machine. Experimental materials used in this study were SUS304L with dimension of 100 × 30 × 1 mm³, for each welding process two plates are joined by the lap joint method. The top plate were perforated with a diameter of 11 mm, then filled with filler to connect the two plates. The dimensions and shape of the specimens can be seen in Figure 1. The electrode used were ER308L-Si with a diameter of 0.8 mm. Shielding gas composition were adjusted by gas mixture (Figure 2).

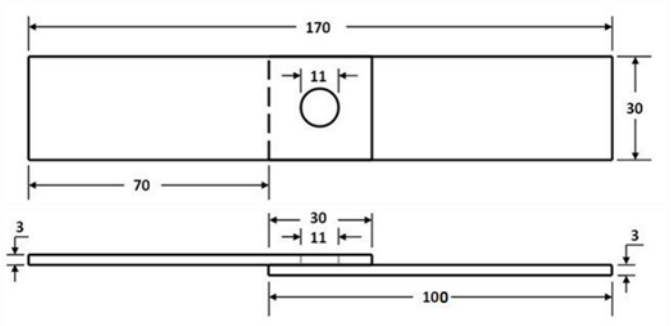

Figure 1: Specimen dimensions (mm) .

Figure 2: Gas Mixture.

Different shielding gas composition: 100% Ar; 92,5% Ar-7,5% CO_2; 85% Ar-15% CO_2 ; 77,5% Ar-22,5% CO_2; 100% CO_2 and welding current of 80 A, 100 A and 120 A at constant time of 5s were used during this experiment. The shielding gas rate in the welding process is 10 l/min.

The tests carried out included observations of microstructure, shear tensile testing and Vickers hardness testing. Shear tensile test based on AWS D8.9-97. Microvickers hardness test based on ASTM E92. Microstructure were observe using a micro microscope with Aqua Regia etching solution consisting of 30 ml HCl and 10 ml HNO_3 impact.

3. RESULT AND DISCUSSION

3.1 Macrostructures and microstructures

Macro photos are used to observe cross-section of nugget on the weld. Nugget is one part of the weld that is formed due to melting of the side of the plate interface that is exposed to heat during the welding process. Based on the observation of macro photos in Figure 3, with increasing welding current, the size of the nugget increases. It is well known that increasing the heat input makes the size of the nugget grows larger [14]. Figure 4 shows that the increase in CO_2 content in the shielding gas causes size of the nugget produced to become larger. CO_2 gas decomposes into CO and O during the welding process, these gas helps the combustion process to be better and increases heat input [15]. The more CO_2 content in the shielding gas makes the heat input increase [7].

Besides showing the formed nuggets, macro photos also show defects in the welding results. These defects are in the form of gap at the bottom edge of the weld area or can be called incomplete fusion (IF) defects. This IF gap were caused by the molten metal was not able to blend perfectly with base metal [16]. This defect is caused by several factors, including welding current, welding speed, and the groove angle or hole filled with molten metal. Too low heat input and short welding time cause the electrodes to not melt completely. The molten metal solidifies first before filling the entire area in the hole that has been made.

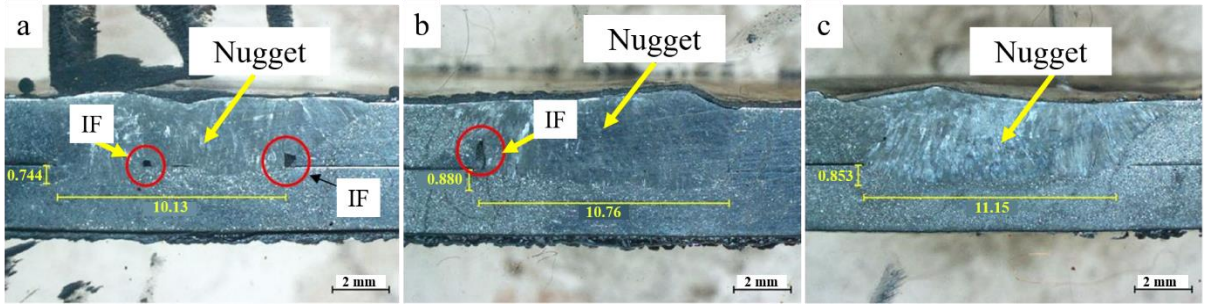

Figure 3: Nugget cross section macro photo of different welding currents: (a). 80 A, (b). 100 A and (c). 120 A (Dimensions in mm).

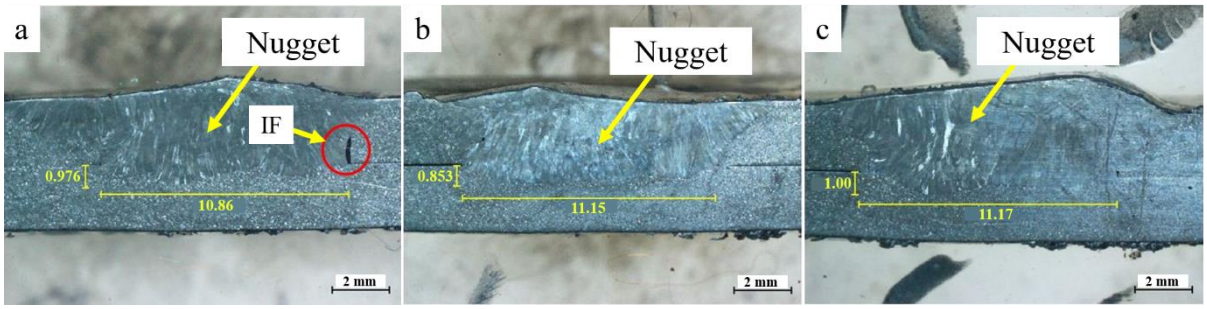

Figure 4: Nugget cross section macro photo of different shielding gas compossition: (a). 7,5% CO_2, (b). 15% CO_2 and (c). 22,5% CO_2 (Dimensions in mm)

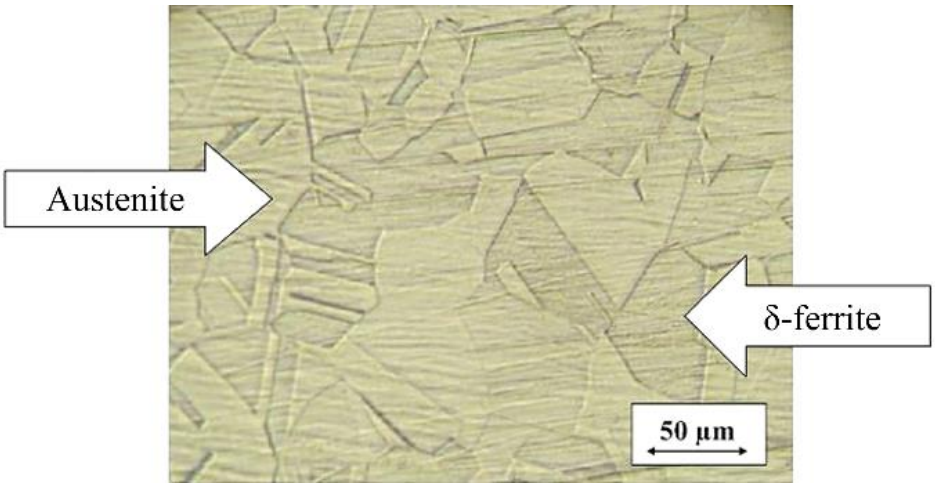

Figure 5: Microstructure of SUS304L base metal.

Microstructure test was carried out to determine the phase that occurred in welded joints. Specimens were etched with Aqua Regia solution for stainless steel. From Figure 5 we can see that the microstructure of the base metal SUS304L is austenite and δ-ferrite phases.

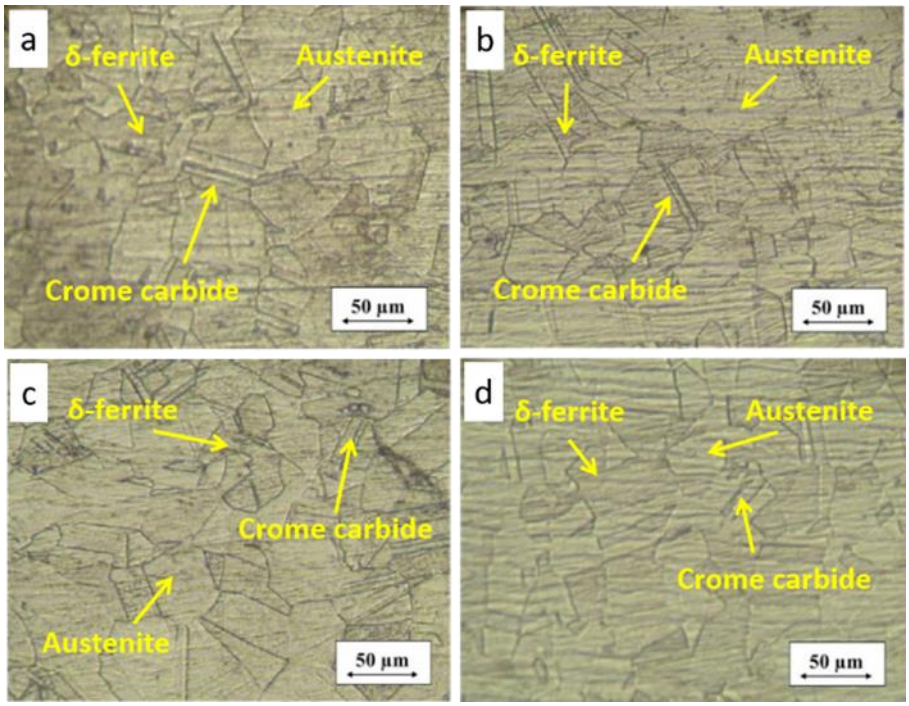

Figure 6: Microstructure of HAZ with 80A welding current: (a). 7,5% CO_2, (b). 15% CO_2, (c). 22,5% CO_2 and (d). 100% CO_2.

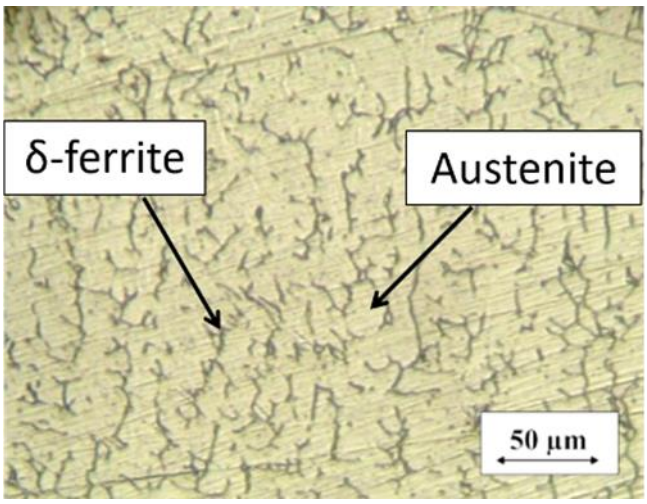

Figure 7: Microstructure of weld metal

During the welding process on stainless steel, chromium carbide formation can occur at the grain boundaries or also known as sensitization. This condition is often found in heat affected zones (HAZ). The formation of Chrome carbide is one of the causes of grain boundary corrosion [17]. Figure 6 shows that the HAZ microstructure consists of austenite and δ-ferrite phases. It also shows that at the grain boundaries a Chrome carbide ($Cr_{23}C_6$) precipitate is formed. SUS304L has less carbon content than SS 304 so the Chrome carbide in SUS304L formed is smaller. The weld area produces a dendritic core structure containing δ-ferrite and austenite, as shown in Figure 7. The δ-ferrite phase is between the dendritic cells. The dendritic core structure is characteristic of the rapid solidification of the austenite phase during the smelting process [18].

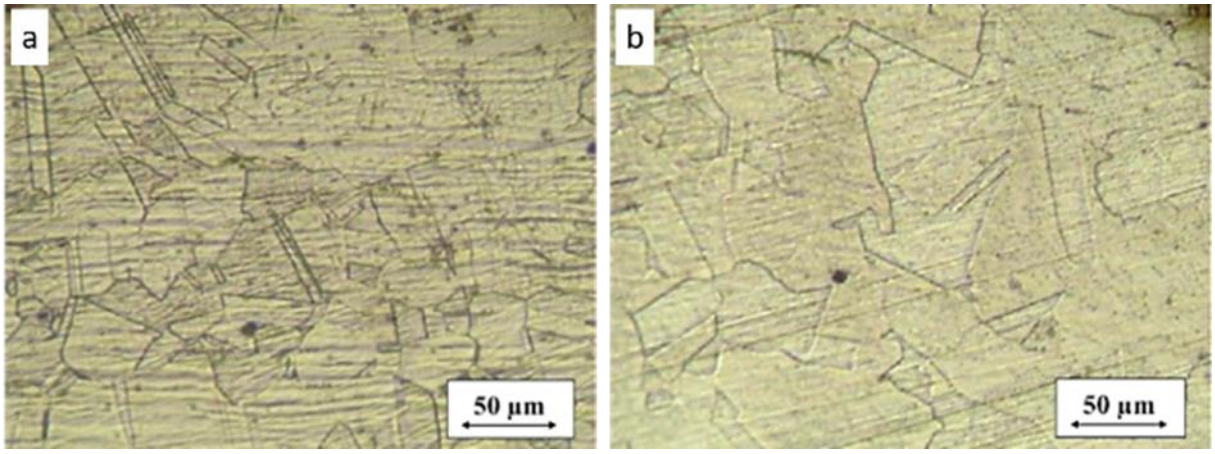

Figure 8: Microstructure of HAZ with shielding gas of 15% CO_2: (a). 80A and (b). 120A

Figure 8 shows the difference in grain size in the variation of welding current. The higher the welding current used, the larger the grains formed. The addition of CO_2 levels in the shielding gas also causes an increase in the size of the grains formed.

Based on the results of micro photos in the weld metal and HAZ, it was found that with increasing welding current and CO_2 content in the shielding gas there was no significant change in all variations. The grain size in these images cannot be determined in plain view, so the grain size calculation is carried out to obtain a number indicating the size of the grains formed.

3.2 Grains calculation

Calculating grain size can be done using the Planimetric method developed by Jeffries. Where this method is quite simple to determine the number of grains per unit area in the plane that can be connected to the ASTM E112 grain size standard. This planimetric method involves the number of grains contained in a certain area which is denoted by N_A. Schematically the calculation process using this method is shown in Figure 9.

The number of items inside the circle (N_{inside}) plus the number of items that are tangent ($N_{intercepted}$) with the circle multiplied by Jeffries multiplier (f) can be written in equation 1. The number of items inside the circle (N_{inside}) plus the number of items that are tangent ($N_{intercepted}$) with the circle multiplied by Jeffries multiplier (f) can be written in equation 1 [17]. Where the Jeffries multiplier used depends on the magnification used when viewing the microstructure and can be determined through Table 1.

$$N_A = f\left(N_{inside} + \frac{N_{intercepted}}{2}\right) \quad \text{..... (1)}$$

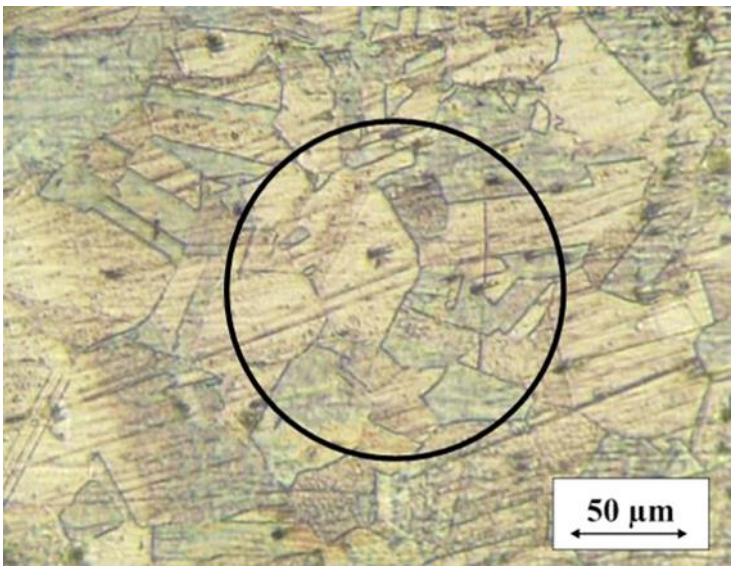

Figure 9: Pattern of grain size calculation using the Planimetric method.

Table 1: The relationship between the magnification used and the Jeffries multiplier .

Magnification (*M*)	**Jeffries multiplier (*f*) to determine grains/mm^2**
1	0,0002
10	0,02
25	0,125
50	0,5
75	1,125
100	2,0
150	4,5
200	8,0
250	12,5
300	18,0
500	50,0
750	112,5
1000	200,0

The results of the calculation of the number of grains can be used to calculate the grain size (G) with equation 2.

$G = [3{,}322 \log(N_A)] - 2{,}95$ ..... (2)

The grain size value (G) is used to find the grain diameter value in the ASTM E112 table. Figure 10 shows the increase in CO_2 content in the shielding gas causes the grain size to increase. CO_2 gas decomposes into CO and O_2 during the welding process, these gases help the combustion process and increase the welding heat input. This causes a slow cooling rate. The faster the cooling rate or the decrease in temperature, the faster grain growth can stop [18]. Grain size affects the mechanical strength of the welding results, the larger the grain, the higher the tensile-shear load [19].

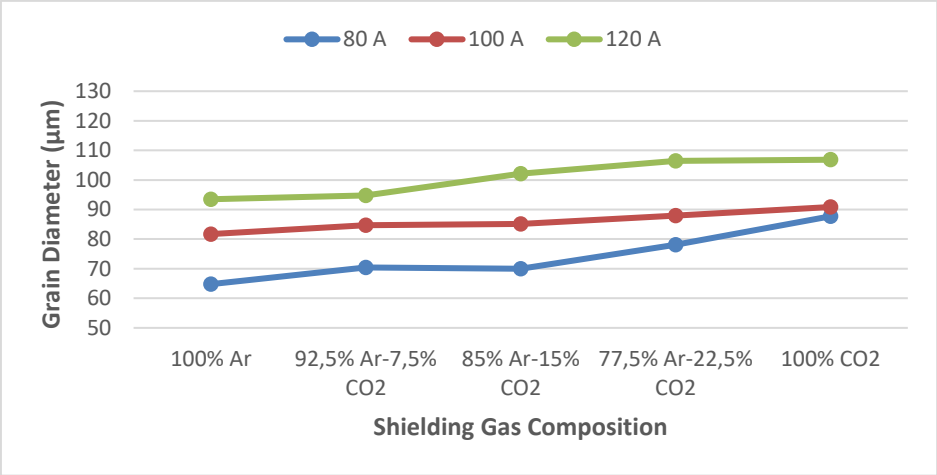

Figure 10: Grain diameter on HAZ region.

3.3 Hardness Test

Vickers hardness test was carried out to determine the hardness of the base metal, HAZ and nuggets. Hardness test refers to ASTM E92 testing standard, a pyramidal diamond indenter with an angle of 136° used for this test. Indenter was pressed with a compressive force of 100 gf for 15 seconds.

The hardness test result showed that the nugget had the highest hardness value compared to HAZ and base metal. Nuggets and HAZ undergo a thermal welding cycle, the greater the heat input in the area, the greater the changes in the microstructure, especially in the grains size. This causes the grains formed in nugget and HAZ to be smaller than base metal area [20]. The highest hardness value occurs in the nugget and weld metal, because it consists of austenite and δ-ferrite in the form of dendrites. The fine grain shape of austenite and δ-ferrite in the weld metal (in Figure 7) also affects the hardness results. Coarse grain shape makes the hardness value decrease [21].

Figure 11 shows the Vickers hardness value at a welding current of 80 A with different shielding gas variations. The highest hardness value in nugget area is successively at the shielding gas variation of 100% Argon; 92,5% Ar-7,5% CO_2; 85% Ar-15% CO_2; 77,5% Ar-22,5% CO_2; and 100% CO_2 were 206,1 HV; 205,3 HV; 201,1 HV; 197,5 HV; and 194,4 HV. The average hardness values in the HAZ area are respectively: 181.95 HV; 182.05 HV; 178.2 HV; 177.4 HV; and 175.55 HV.

Figure 12 shows the Vickers hardness value at a welding current of 100 A with different shielding gas variations. The highest hardness value in the nugget area is successively at the shielding gas variation of 100% Ar; 92,5% Ar-7,5% CO_2; 85% Ar-15% CO_2; 77,5% Ar-22,5% CO_2; and 100% CO_2 were 191,6 HV; 189,8 HV; 185,6 HV; 185,8 HV; and 183,7 HV. The average hardness values in the HAZ area are respectively: 173.15 HV; 172.9 HV; 171.4 HV; 170.1 HV; and 168.95 HV.

Figure 13 shows the Vickers hardness value at a welding current of 120 A with different shielding gas variations. The highest hardness value in nugget area is successively at the shielding gas variation of 100% Argon; 92,5% Ar-7,5% CO_2; 85% Ar-15% CO_2; 77,5% Ar-22,5% CO_2; dan 100% CO_2 adalah 187,3 HV; 185,5 HV; 182,7 HV; 181,7 HV; dan 179,5 HV. The average hardness values in the HAZ area are respectively: 171,7 HV; 170,7 HV; 166,9 HV; 166,3 HV; and 164,4 HV.

Welding current affects the hardness of the specimen. As shown by Figure 9; Figure 10 and Figure 11, the lower the welding current, the greater the hardness value. This is in line with expectations because the welding current affects the heat input in the welding process. The higher the heat input, the lower the hardness value

Hardness test results in Figure 11; Figure 12; and Figure 13 shows that the shielding gas composition of 100% Argon has the highest hardness compared to other gas compositions. This is because Argon gas during welding causes a quenching effect. Rapid heat loss occurs in weld metal because it receives the highest heat input, then heat is transferred through argon gas. Higher heat coefficient of shielding gas causes the cooling rate to occur faster [15], [22]. This is in accordance with the Jominy test, areas that experience foremost cooling will get the highest hardness values [23].

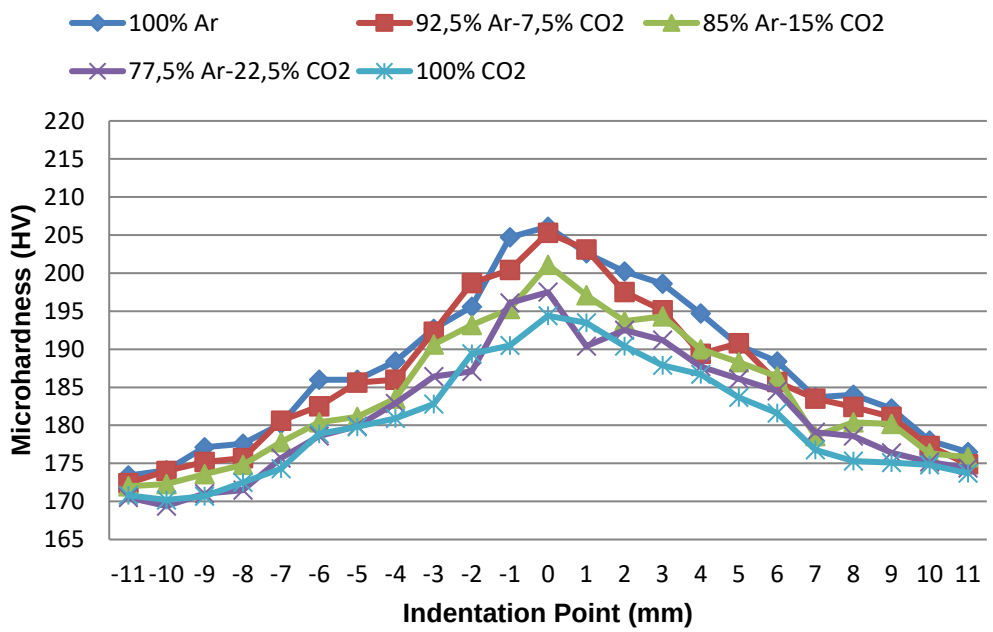

Figure 11: Microhardness of welding result using shielding gas variations with 80 A welding current.

Microhardness results on the weld metal decrease along with the increase in CO_2 percentage, this is also evidence that CO_2 cooling rate of is slower than Ar gas. Large grains are formed due to the slow cooling rate, this causes a decrease in hardness. The greater CO_2 content in shielding gas delivers slow cooling rate and high heat input.

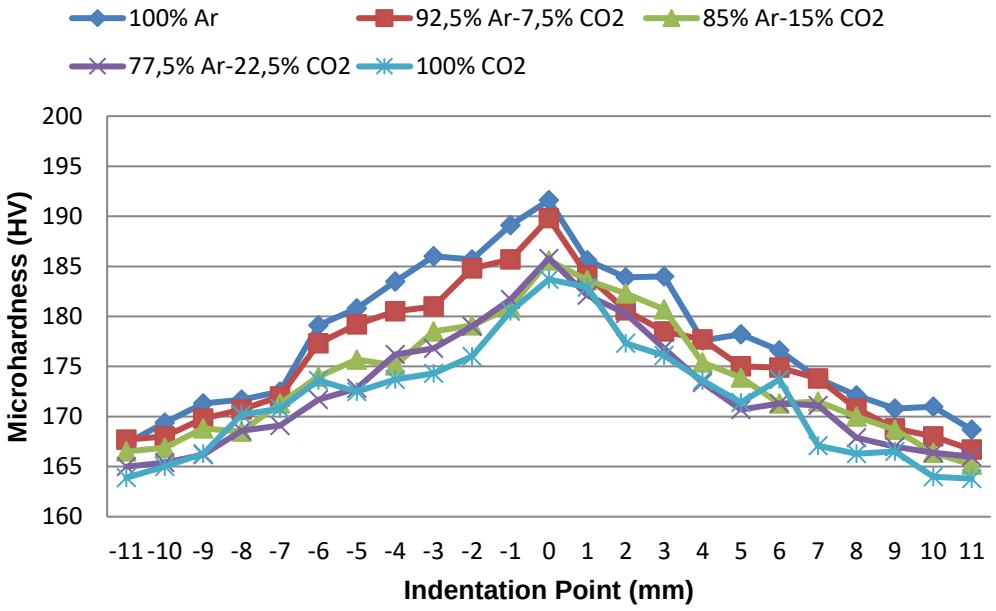

Figure 12: Microhardness of welding result using shielding gas variations with 100 A welding current.

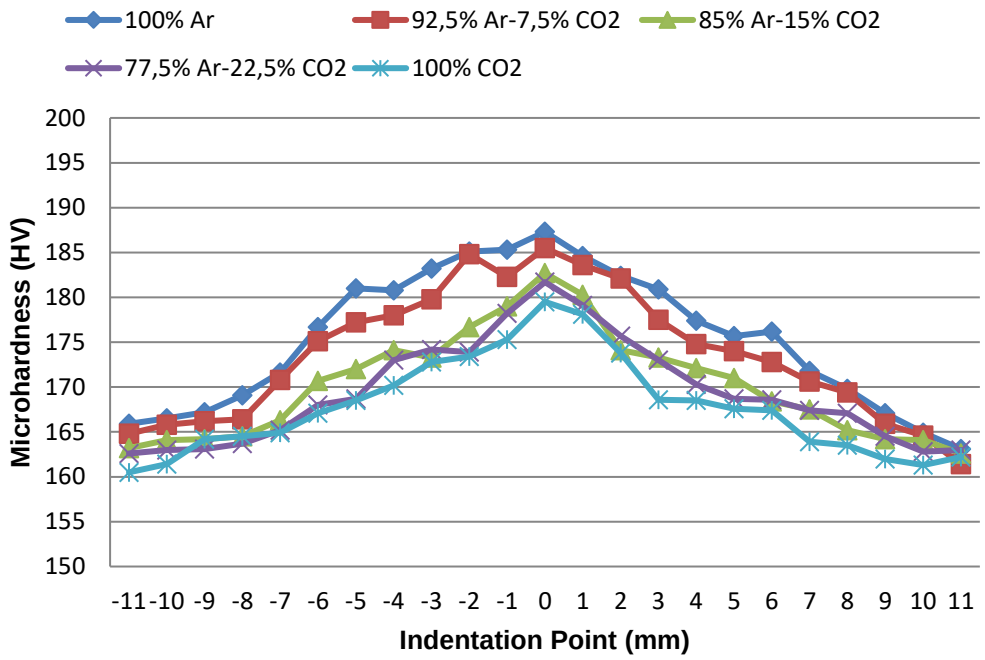

Figure 13: Microhardness of welding result using shielding gas variations with 120 A welding current.

3.4 Shear Tensile Test

Shear tensile test was carried out to determine the mechanical properties of the welds in the form of maximum tensile-shear load carrying capacity and failure modes that occur. Tests were performed using the AWS D8.9 standard. The results showed that the welding current and shielding gas composition had an effect on tensile strength of the welded joint.

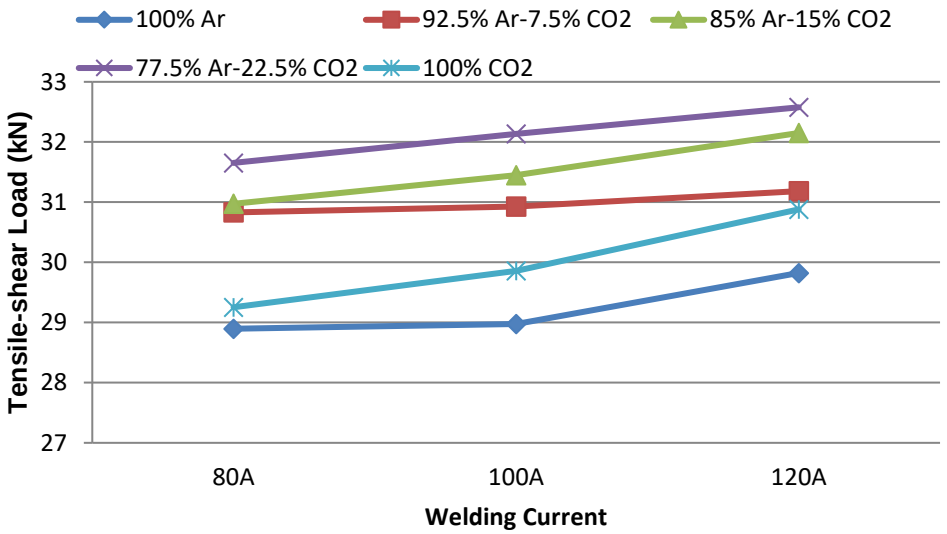

Figure 14: Tensile-shear strength test result using variation of welding current and shielding gas compositions.

Tensile-shear strength of welding result are shown in Figure 14. The highest value of Tensile-shear strength was obtained at 120 A welding current. Shear-tensile load increases with increasing welding current used. These results are directly proportional to Alizadeh-Sh's research in 2014, that an increase in tensile load occurs due to an increase in welding current [24]. This is because welding current greatly affects heat input at welding process. The high heat input causes cooling rate after welding process becomes slower, resulting in formation of large grains.

The highest shear-tensile load was obtained with a shielding gas composition of 77,5% Ar - 22,5% CO_2. Kah in 2013 [25] has investigated the formation of ferrite in welding results with a mixture of Ar and CO_2 shielding gases, the result is that Ar gas produces acicular ferrite (AF) and CO_2 delivers a slow cooling rate. This happens because Ar percentage in shielding gas affects the amount of ferrite in welding result [26]. Therefore, the combination of Ar and CO_2 is balanced because the formation of ferrite and large grains increases the strength of the welded joint. These results are in accordance with this study because when Ar and CO_2 gases are combined, the results will be better than 100% by each gas.

Figure 14 also shows that the shear-tensile load increases with increasing CO_2 content. This further confirms that CO_2 content in the shielding gas composition affects the heat input during welding process. CO_2 gas contained in the shielding gas during welding process decomposes into CO and O_2 which will help the combustion process and icrease the heat input [27]–[29].

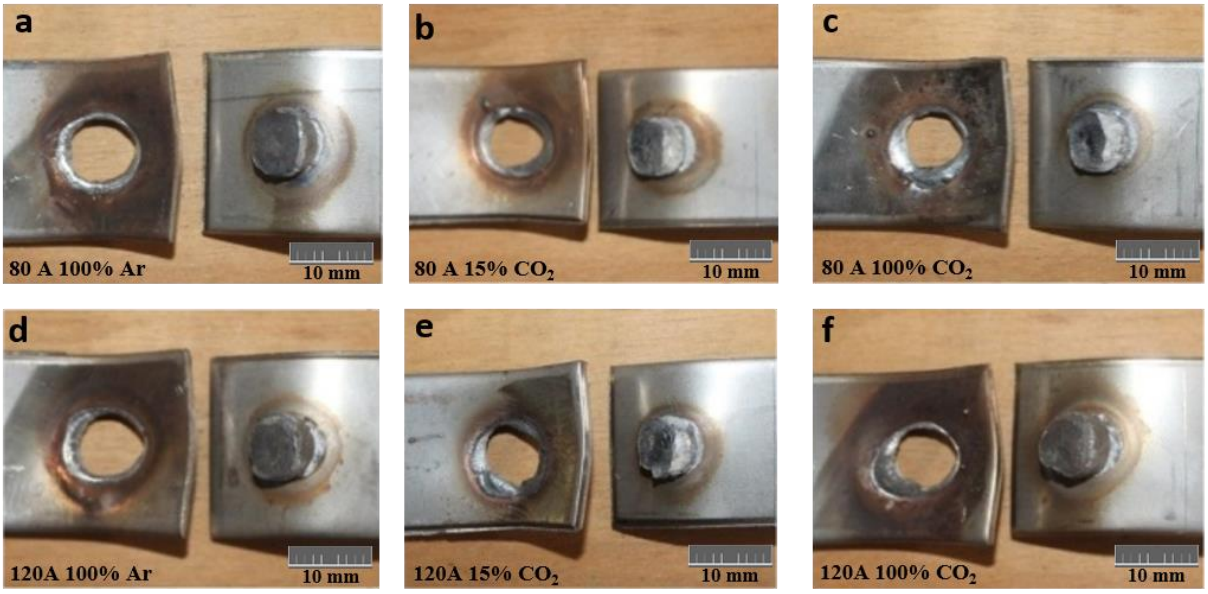

Figure 15: Specimen fracture of tensile-shear test results.

Figure 15 shows fracture that occurs from tensile-shear test. All variations deliver a pull out fracture form. This failure occurs due to damage to the area around the weld area so that the plate is damaged and the plate is torn. This failure can occur because weld metal has a higher tensile-shear strength than it's surrounding area, then in the tensile-shear test failure start and occurs in the area around the weld (the weakest). Pull out failure is the type of failure expected by engineers because it has the ability to withstand higher loads than base metal.

4. CONCLUSION

1. The microstructure in the nugget region is a dendritic structure consisting of austenite and δ –ferrite. The increase in welding current and CO_2 content in the shielding gas causes an increase in grain size in the HAZ region.
2. The highest hardness value is found in the nugget area. The variation of the protective gas composition with the highest hardness value is 100% Argon with a welding current of 80 A. This is because the area that experiences the fastest cooling rate will get the highest hardness value.
3. The highest shear-tensile load was obtained on specimens with shielding gas of 77.5% Ar-22.5% CO_2 at a welding current of 120 A. The size of the nugget and welding defects affected the value of the tensile-shear load.

5. SUGGESTION

Based on the research that has been done, the suggestion that can be given in the next research is plug welding research using different plate thickness variations, to get maximum strength on the specimen. This can be done by estimating the variation in which interfacial and pullout failures will occur.

6. REFERENCES

[1] R. RAHARJO, N. HAMIDI, T. D. WIDODO, R. BINTARTO, and E. HABIBULFALAH, "Pengaruh clamping frame kayu meranti dan ASTM A36 pada friction spot joining Al 1100 dan PVC," Rekayasa Mesin, vol. 11, no. 2, pp. 257–265, 2020, doi: https://doi.org/10.21776/ub.jrm.2020.011.02.12.

[2] M. SOKOLUK, C. CAO, S. PAN, and X. LI, "Nanoparticle-enabled phase control for arc welding of unweldable aluminum alloy 7075," *Nat. Commun.*, vol. 10, no. 98, pp. 1–8, 2019, doi: 10.1038/s41467-018-07989-y.

[3] I. BITHARAS, N. A. MCPHERSON, W. MCGHIE, D. ROY, and A. J. MOORE, "Visualisation and optimisation of shielding gas coverage during gas metal arc welding," *J. Mater. Process. Technol.*, vol. 255, no. October 2017, pp. 451–462, 2018, doi: 10.1016/j.jmatprotec.2017.11.048.

[4] M. NADYA, Y. S. IRAWAN, and M. A. CHOIRON, "Pengaruh double chamfer terhadap distribusi suhu dan daerah Zpl pada sambungan las gesek Al 6061 dengan simulasi komputer," Rekayasa Mesin, vol. 11, no. 2, pp. 433–445, 2021, doi: https://doi.org/10.21776/ub.jrm.2021.012.02.20.

[5] J. F. TU and A. G. PALEOCRASSAS, "Fatigue crack fusion in thin-sheet aluminum alloys AA7075-T6 using low-speed fiber laser welding," *J. Mater. Process. Technol.*, vol. 211, pp. 95–102, 2011, doi: 10.1016/j.jmatprotec.2010.09.001.

[6] L. PELLONE, G. INAMKE, K. HONG, and Y. C. SHIN, "Effects of interface gap and shielding gas on the quality of alloy AA6061 fiber laser lap weldings," *J. Mater. Process. Tech.*, vol. 268, no. October 2018, pp. 201–212, 2019, doi: 10.1016/j.jmatprotec.2019.01.025.

[7] R. KAÇAR and K. KÖKEMLI, "Effect of controlled atmosphere on the mig-mag arc weldment properties," *Mater. Des.*, vol. 26, no. 6, pp. 508–516, 2005, doi: 10.1016/j.matdes.2004.07.027.

[8] Y. XIE and J. ZHANG, "Chloride-induced stress corrosion cracking of used nuclear fuel welded stainless steel canisters: A review," *J. Nucl. Mater.*, vol. 466, pp. 85–93, 2015, doi: 10.1016/j.jnucmat.2015.07.043.

[9] M. TANAKA, S. TASHIRO, M. USHIO, T. MITA, A. B. MURPHY, and J. J. LOWKE, "CO2-shielded arc as a high-intensity heat source," *Vacuum*, vol. 80, no. 11–12, pp. 1195–1198, 2006, doi: 10.1016/j.vacuum.2006.01.047.

[10] V. A. SETYOWATI, SUHENI, F. ABDUL, and S. ARIYADI, "Effect of welding methods for different carbon content of ss304 and ss304l materials on the mechanical properties and microstructure," *IOP Conf. Ser. Mater. Sci. Eng.*, vol. 1010, no. 1, 2021, doi: 10.1088/1757-899X/1010/1/012018.

[11] R. R. AMBRIZ, G. BARRERA, R. GARCÍA, and V. H. LÓPEZ, "A comparative study of the mechanical properties of 6061-T6 GMA welds obtained by the indirect electric arc (IEA) and the modified indirect electric arc (MIEA)," *Mater. Des.*, vol. 30, no. 7, pp. 2446–2453, 2009, doi: 10.1016/j.matdes.2008.10.025.

[12] P. E. SETYAWAN, Y. S. IRAWAN, and W. SUPRAPTO, "Kekuatan Tarik Dan Porositas Hasil Sambungan Las Gesek Aluminium 6061 Dengan Berbagai Suhu Aging," Rekayasa Mesin, vol. 5, no. 2, p. pp.141-148, 2014, doi: 10.21776/ub.jrm.

[13] V. I. VISHNYAKOV, S. A. KIRO, M. V. OPRYA, and A. A. ENNAN, "Effect of shielding gas temperature on the welding fume particle formation: Theoretical model," *J. Aerosol Sci.*, vol. 124, pp. 112–121, 2018, doi: 10.1016/j.jaerosci.2018.07.006.

[14] Y. R. WONG and S. F. LING, "An investigation of dynamical metal transfer in GMAW - Effects of argon shielding gas," *J. Mater. Process. Technol.*, vol. 214, no. 1, pp. 106–111, 2014, doi: 10.1016/j.jmatprotec.2013.08.003.

[15] L. L. WANG, F. G. LU, H. P. WANG, A. B. MURPHY, and X. H. TANG, "Effects of shielding gas composition on arc profile and molten pool dynamics in gas metal arc welding of steels," *J. Phys. D. Appl. Phys.*, vol. 47, no. 46, 2014, doi: 10.1088/0022-3727/47/46/465202.

[16] Y. OGINO, Y. HIRATA, and A. B. MURPHY, "Numerical simulation of GMAW process using Ar and an Ar–CO2 gas mixture," *Weld. World*, vol. 60, no. 2, pp. 345–353, 2016, doi: 10.1007/s40194-015-0287-3.

[17] A. MURTIONO, "Pengaruh quenching dan tempering terhadap kekerasan dan kekuatan tarik serta struktur mikro baja karbon sedang untuk mata pisau pemanen sawit," *e-Dinamis*, vol. II, no. 2, 2012.

[18] C. RAJARAJAN, P. SIVARAJ, and V. BALASUBRAMANIAN, "Microstructural analysis of weld nugget properties on resistance spot-welded advance high strength dual phase (α+α /) steel joints," *Mater. Res. Express*, vol. 7, no. 1, 2020, doi: 10.1088/2053-1591/ab654d.

[19] I. GUZMÁN, E. GRANDA, B. VARGAS, C. CRUZ, Y. AVILA, and J. ACEVEDO, "Tensile and fracture behavior in 6061-T6 and 6061-T4 aluminum alloys welded by pulsed metal transfer GMAW," *Int. J. Adv. Manuf. Technol.*, vol. 103, no. 5–8, pp. 2553–2562, 2019, doi: 10.1007/s00170-019-03673-7.

[20] M. SHOME, "Effect of heat-input on austenite grain size in the heat-affected zone of HSLA-100 steel," *Mater. Sci. Eng. A*, vol. 445–446, pp. 454–460, 2007, doi: 10.1016/j.msea.2006.09.085.

[21] V. V. SATYANARAYANA, G. M. REDDY, and T. MOHANDAS, "Dissimilar metal friction welding of austenitic-ferritic stainless steels," *J. Mater. Process. Technol.*, vol. 160, no. 2, pp. 128–137, 2005, doi: 10.1016/j.jmatprotec.2004.05.017.

[22] S. LU, H. FUJII, and K. NOGI, "Weld shape variation and electrode oxidation behavior under Ar-(Ar-CO2) double shielded GTA welding," *J. Mater. Sci. Technol.*, vol. 26, no. 2, pp. 170–176, 2010, doi: 10.1016/S1005-0302(10)60028-X.

[23] J. S. ZUBACK and T. DEBROY, "The hardness of additively manufactured alloys," *Materials (Basel).*, vol. 11, no. 11, 2018, doi: 10.3390/ma11112070.

[24] M. ALIZADEH-SH, S. P. H. MARASHI, and M. POURANVARI, "Resistance spot welding of AISI 430 ferritic stainless steel: Phase transformations and mechanical properties," *Mater. Des.*, vol. 56, pp. 258–263, 2014, doi: 10.1016/j.matdes.2013.11.022.

[25] P. KAH and J. MARTIKAINEN, "Influence of shielding gases in the welding of metals," *Int. J. Adv. Manuf. Technol.*, vol. 64, no. 9–12, pp. 1411–1421, 2013, doi: 10.1007/s00170-012-4111-6.

[26] D. KATHERASAN, P. SATHIYA, and A. RAJA, "Shielding gas effects on flux cored arc welding of AISI 316L (N) austenitic stainless steel joints," *Mater. Des.*, vol. 45, pp. 43–51, 2013, doi: 10.1016/j.matdes.2012.09.012.

[27] G. CAMPANA, A. ASCARI, A. FORTUNATO, and G. TANI, "Hybrid laser-MIG welding of aluminum alloys: The influence of shielding gases," *Appl. Surf. Sci.*, vol. 255, no. 10, pp. 5588–5590, 2009, doi: 10.1016/j.apsusc.2008.07.169.

[28] L. ZHAO, T. SUGINO, G. ARAKANE, and S. TSUKAMOTO, "Influence of welding parameters on distribution of wire feeding elements in CO2 laser GMA hybrid welding," *Sci. Technol. Weld. Join.*, vol. 14, no. 5, pp. 457–467, 2009, doi: 10.1179/136217109X434252.

[29] L. ZHAO, S. TSUKAMOTO, G. ARAKANE, T. SUGINO, and T. DEBROY, "Influence of oxygen on weld geometry in fibre laser and fibre laser-GMA hybrid welding," *Sci. Technol. Weld. Join.*, vol. 16, no. 2, pp. 166–173, 2011, doi: 10.1179/1362171810Y.0000000010.